

Arabinose Alters Both Local and Distal H–D Exchange Rates in the *Escherichia coli* AraC Transcriptional Regulator

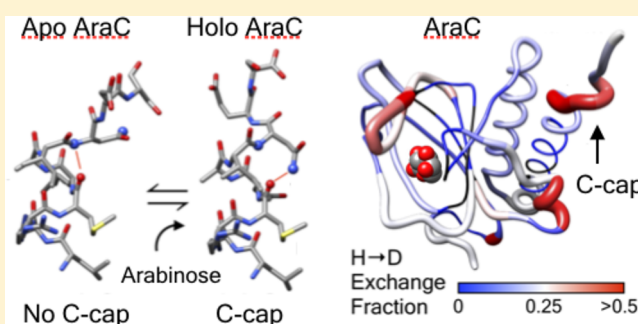
Alexander Tischer,[†] Matthew J. Brown,[‡] Robert F. Schleif,^{*,‡} and Matthew Auton^{*,†}

[†]Division of Hematology, Departments of Internal Medicine and Biochemistry and Molecular Biology, Mayo Clinic, Rochester, Minnesota 55905, United States

[‡]Department of Biology, Johns Hopkins University, Baltimore, Maryland 21218, United States

S Supporting Information

ABSTRACT: In the absence of arabinose, the dimeric *Escherichia coli* regulatory protein of the L-arabinose operon, AraC, represses expression by looping the DNA between distant half-sites. Binding of arabinose to the dimerization domains forces AraC to preferentially bind two adjacent DNA half-sites, which stimulates RNA polymerase transcription of the *araBAD* catabolism genes. Prior genetic and biochemical studies hypothesized that arabinose allosterically induces a helix–coil transition of a linker between the dimerization and DNA binding domains that switches the AraC conformation to an inducing state [Brown, M. J., and Schleif, R. F. (2019) *Biochemistry*, preceding paper in this issue (DOI: 10.1021/acs.biochem.9b00234)]. To test this hypothesis, hydrogen–deuterium exchange mass spectrometry was utilized to identify structural regions involved in the conformational activation of AraC by arabinose. Comparison of the hydrogen–deuterium exchange kinetics of individual dimeric dimerization domains and the full-length dimeric AraC protein in the presence and absence of arabinose reveals a prominent arabinose-induced destabilization of the amide hydrogen-bonded structure of linker residues (I₁₆₇ and N₁₆₈). This destabilization is demonstrated to result from an increased probability to form a helix capping motif at the C-terminal end of the dimerizing α -helix of the dimerization domain that precedes the interdomain linker. These conformational changes could allow for quaternary repositioning of the DNA binding domains required for induction of the *araBAD* promoter through rotation of peptide backbone dihedral angles of just a couple of residues. Subtle changes in exchange rates are also visible around the arabinose binding pocket and in the DNA binding domain.



The homodimeric *Escherichia coli* protein, AraC,^{2–4} regulates transcription of the *araBAD* genes required for the catabolism of L-arabinose as well as the *araC* gene itself.⁵ The *araBAD* genes and the *araC* gene are transcribed in opposite directions yielding mRNAs that are translated into the enzymes required for arabinose catabolism and the AraC gene regulator (Figure 1A).⁶ AraC consists of a dimerization domain that binds arabinose^{7,8} and a DNA binding domain⁹ connected by an interdomain linker.^{10,11} Regulation of the arabinose operon is achieved by the binding of arabinose to AraC, which facilitates its switching from a repressor to an activator of transcription involving five DNA binding half-sites, the adjacent I₁ and I₂ half-sites of *araI*, 35 bp upstream of the *p*_{BAD} transcription start site, two half-sites at *araO*₁ 120 bp upstream of *p*_{BAD}, and the half-site at *araO*₂ that is 245 bp upstream of *p*_{BAD}.¹²

In the absence of arabinose, AraC predominantly loops the DNA between I₁ and O₂ and represses the transcription of both the genes encoding itself and the catabolic enzymes.¹³ AraC can also autoregulate its own synthesis in the presence of arabinose by binding to the adjacent half-sites of O₁ that overlap the pC RNA polymerase binding region.^{14–16} The

repressed state involving DNA looping is dependent on supercoiling of the bacterial DNA.^{17,18} The binding of arabinose to the dimerization domains causes AraC to switch from a DNA looped O₂–I₁ bound configuration to an unlooped configuration in which AraC binds the adjacent *araI* sites, I₁ and I₂ (Figure 1A).¹⁹ This unlooped DNA state stimulates RNA polymerase to bind and initiate transcription from *p*_{BAD}.

The shift from repressing to inducing requires a substantial quaternary structural rearrangement of the domains of AraC (Figure 1A).¹⁹ Many of the recent studies of AraC have been directed at understanding the mechanisms by which the binding of arabinose brings about these structural changes.^{20–22} The binding of arabinose to the protein's dimerization domains has been proposed to reduce the rigidity with which the DNA binding domains are held in positions and orientations favoring DNA looping. A more flexible state of the protein reduces the energetic cost of repositioning the

Received: April 30, 2019

Revised: June 12, 2019

Published: June 14, 2019

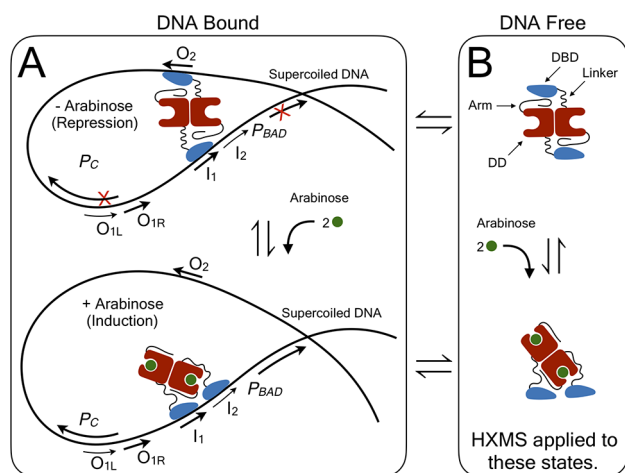


Figure 1. Thermodynamic cycle illustrating the binding of arabinose to AraC in DNA-bound and free states. (A) Arabinose-induced light switch mechanism between the DNA looped repressed state and the unlooped activated state. (B) Arabinose-induced conformational selection in the absence of DNA. HXMS is applied to these conformational states.

DNA binding domains required for binding to adjacent DNA half-sites, and much of the repressed, DNA looped, species is then replaced by DNA with AraC bound at I_1 – I_2 .¹⁶ Two regions of AraC have been implicated to be involved in such a structural rearrangement.

(1) Crystallographic structures of the dimerization domain with and without bound arabinose show the N-terminal arm (first 20 residues of AraC) in two different conformations.^{9,23} The binding of arabinose repositions the arm so that it binds directly over the bound arabinose. This conformational change has been proposed to be the first step of a mechanism that changes the protein's flexibility. Consistent with this notion is the fact that almost all of the mutations that weaken repression by AraC lie in the arms.^{24,25} Deletions also reduce or eliminate repression.²² These facts imply that in the absence of arabinose, the arm plays a key role in holding the protein in its less flexible, repressing state and that the arm's repositioning in the presence of arabinose terminates this activity.²⁰

(2) The second region that appears to be involved in the repression-inducing conformational shift of AraC is the eight-residue linker¹¹ between the dimerization domain and the DNA binding domain. This linker is malleable with respect to mutations it can accommodate,¹⁰ but recent studies suggest it plays an active role in AraC's conformational switch. Mutations in this region that weaken repression, enhance induction of p_{BAD} , and possibly alter the DNA half-site binding preference have been identified.²⁶ Fluorescence anisotropy measurements have also shown that binding of arabinose to AraC lacking the DNA binding domains increases the flexibility of the linker.²⁷ Furthermore, recent studies substituting polyalanine or polyglycine into the linker and insertions and deletions in the linker indicate that in the absence of arabinose, the linker may be helical and lead to the hypothesis that the addition of arabinose destabilizes the helix,¹ a hypothesis which motivated the studies presented here.

Here, we query the arabinose free and arabinose-bound states of AraC in the absence of DNA using HXMS on the assumption that the properties of AraC relevant to its conformational shift in the presence of arabinose (Figure 1B) can be observed in the absence of DNA. HXMS²⁸

measures the steady-state time-dependent accumulation of deuterium in the peptide backbone. When diluted into $^2\text{H}_2\text{O}$ buffer, protein amide hydrogens exchange with solvent deuterium according to the local conformational dynamics of the peptide backbone. Structurally protected amide hydrogens in a stable H-bonded secondary structure (α -helix or β -sheet) exchange slowly, while amides in flexible regions of structure exchange quickly.

Arabinose binding predominantly increases the amide exchange rates of residues Ile₁₆₇ and Asn₁₆₈ following the C-terminal $\alpha 2$ helix of the dimerization domain near the beginning of the interdomain linker. Contrary to the proposed order to disorder helix–coil transition of this linker,¹ the observed changes instead support a mechanism whereby arabinose binding destabilizes the junction between the dimerizing helix and interdomain linker possibly through the formation of a C-terminal helix cap. Additionally, arabinose stabilizes both the dimerization domains in regions adjacent to the arabinose binding site and the DNA binding domains in the central $\alpha 4$ helices, demonstrating that the DNA binding domains indeed respond to the allosteric effect of arabinose on the interdomain linker even in the absence of DNA.

METHODS

Protein Expression and Purification. Full-length AraC and the dimerization domain were overproduced by the pET24 expression vector (Novagen), isolating the protein by sequential heparin and HiTrap-Q ion exchange columns as previously described.²⁹ The AraC dimerization domain was overproduced by the pET21 expression vector using the first 182 residues of the AraC protein with a C-terminal His6 tag, isolated using a Ni-NTA column and trypsin digestion, followed by a HiTrap-Q column as previously described.²³ Both protein expression constructs have the interdomain linker present.

Hydrogen–Deuterium Exchange Mass Spectrometry (HXMS). HXMS was performed on a Thermo Scientific LTQ Orbitrap XL mass spectrometer coupled to a Waters Nano Acquity UPLC system. HX samples were prepared by dilution of 100 μL of a protein solution [$\sim 20 \mu\text{M}$ AraC dimerization domain in Tris-buffered saline (pH 7.4) with or without 20 mM L-arabinose] into 400 μL of D_2O buffer [TBS (pD 7.4) with or without 20 mM L-arabinose]. Samples were mixed, and the exchange was quenched by a drop in pH to 2.7 at defined time points ranging from 10 s to overnight incubation. Quenched samples were mixed again and injected into a 200 μL loop within the cooling box containing the LC setup at $\sim 0^\circ\text{C}$. After manual injection, the protein was passed through a custom packed pepsin column (250 μL)³⁰ for nonspecific digestion at a flow rate of 200 $\mu\text{L}/\text{min}$ using 0.1% formic acid (pH 2.7). Peptides were collected on a Higgins Analytical Targa C8 trap column. After 5 min, a second valve was used to switch the trap column from an isocratic flow in line with a water/acetonitrile gradient (2 $\mu\text{L}/\text{min}$, 1 to 40% acetonitrile in 18 min, followed by a steep gradient to 90% in 2 min). The gradient elutes peptides from the trap column, while a subsequent Waters Symmetry C18 column separates them prior to injection into the electrospray emitter of the mass spectrometer. The mass spectrometer was operated in positive polarity mode at a resolution of 60000.

Prior to the measurement of HD exchange kinetics, an initial peptide mapping of the AraC dimerization domain and full-length AraC (see Figure S1) was performed using protein

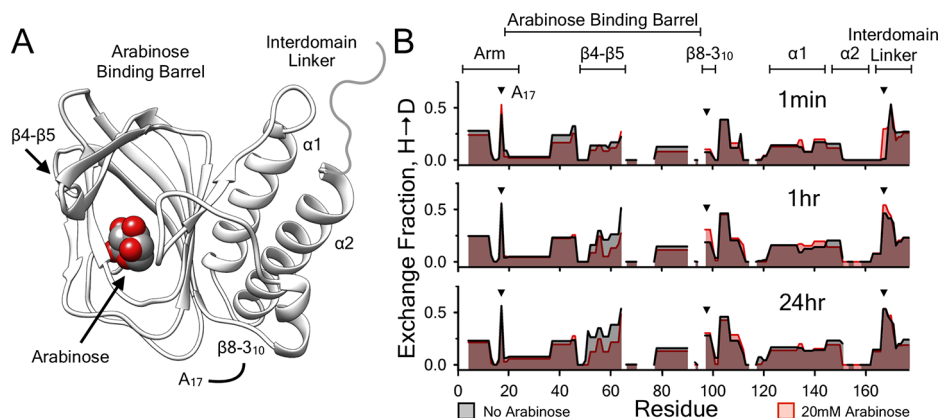


Figure 2. (A) Structure of the AraC dimerization domain (PDB entry 2ARC⁸) highlighting the secondary structures that respond to arabinose binding. Rendered using UCSF Chimera.⁴³ (B) Comparison of the hydrogen exchange of the AraC dimerization domain in the presence (red) and absence (black) of 20 mM arabinose as a function of residue number throughout the protein at three exchange time points, 1 min (top), 1 h (middle), and 24 h (bottom). HXMS was quantified in triplicate at each exchange time point. The majority of AraC hydrogen exchange is unchanged upon binding arabinose. Structural regions that show a kinetic structural effect of binding (see Figures 3–5) are indicated by horizontal bars. The exchange kinetics are quenched by arabinose binding in the arabinose binding barrel containing the $\beta 4$ – $\beta 5$ hairpin loop. The exchange kinetics are enhanced in the $\beta 8$ – $\beta 10$ loop of the arabinose binding barrel connected through space to A₁₇ in the N-terminal arm. The exchange kinetics are also enhanced in the allosteric C-terminal interdomain linker containing residues I₁₆₇ and N₁₆₈.

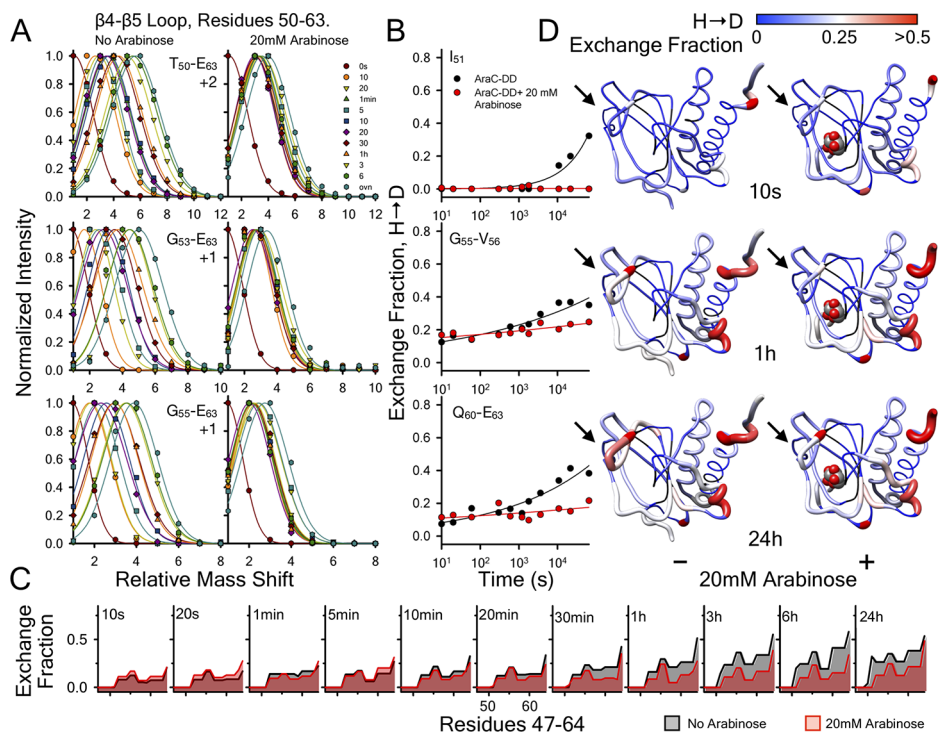


Figure 3. Arabinose binding quenches hydrogen exchange within the $\beta 4$ – $\beta 5$ loop of the dimerization domain near the arabinose binding pocket. HXMS was quantified in triplicate at times between 10 s to 6 h and 24 h. (A) Peptide envelopes (normalized intensity vs mass shift relative to the “all H” peak) of three peptides covering residues 50–63: top, T₅₀–E₆₃, charge state of +2; middle, G₅₃–E₆₃, charge state of +1; bottom, G₅₅–E₆₃, charge state of +1. Relative to the “all H” peptide at time zero, the level of HX is observed to continually increase as a function of time in the absence of arabinose, whereas the overall level of HX of these peptides remains fairly constant as a function of time in the presence of arabinose. (B) Kinetics of HX (exchange fraction vs time) within site-resolved regions of the $\beta 4$ – $\beta 5$ loop: top, I₅₁; middle, G₅₅ and V₅₆; bottom, Q₆₀–E₆₃. (C) Site resolution of the HX exchange fraction vs residue number. Quenching of HX (in panels B and C) is primarily observed at longer incubation times between 30 min and 24 h. (D) Hydrogen–deuterium exchange fraction mapped onto the structure of apo-AraC (PDB entry 1XJA²³) and holo-AraC (PDB entry 2ARC⁸): black, not resolved; blue, 0; white, 0.25; red, ≥ 0.5 . Rendered using UCSF Chimera.⁴³ Arrows indicate the structural location of the $\beta 4$ – $\beta 5$ loop.

dialyzed into 0.1% formic acid (pH 2.7). Multiple “all H” runs were performed using exclusion lists containing well-defined and strong peptide peaks. This procedure provides a more complete peptide map of the protein as it allows the

determination of weaker, less populated peptides. Peptides were identified using Bioworks 3.3.1 (Thermo Fisher Scientific) using a search tolerance of 4 ppm. Exclusion lists were generated with EXMS2³¹ using peptides with a PPe

score of ≥ 0.5 . The final peptide map was generated by combining all successfully identified peptides using a PPe score of ≥ 0.99 .

EXMS2³¹ was used to identify deuterated peptides using the peptide map. The m/z tolerance was 10 ppm, and the retention time window was 4 min for the “all H” sample and 2 min for deuterated samples. The individual and summed peak noise thresholds were set to 500 and 1500, respectively. HDsite³² was performed using an experimental temperature of 25 °C and a pD of 7.4. The deuteration range was set to 0–0.8. Switchable peptides were averaged manually after analysis.

RESULTS

Hydrogen–Deuterium Exchange of the Dimerization Domain.

HXMS was performed on the AraC dimerization domain at a concentration of 20 μM in the presence and absence of 20 mM arabinose (1000-fold excess) to compare the dynamics of AraC in its apo and arabinose-bound states. The affinity of AraC for arabinose (K_D) has been previously determined to be $0.3 \pm 0.03 \mu\text{M}$.^{26,29} In the study presented here, the dimerization domain in its apo and bound states exists as a dimer as at even at picomolar AraC concentrations, the protein remains dimeric.³³

The structure of the AraC dimerization domain (Figure 2A) consists of 10 β -strands that loop around to make up the arabinose binding barrel.⁸ This binding barrel is flanked by a 3_{10} helix and two consecutive antiparallel C-terminal α -helices (residues E₁₂₄–I₁₆₇) that form the dimerization interface. The first residue of the interdomain linker connecting the dimerization domain to the DNA binding domain immediately follows the second helix, $\alpha 2$.²⁶

Figure 2B illustrates the exchange fraction of deuterium incorporated into the arabinose-bound and free states of the dimerization domain at three D₂O incubation times (1 min, 1 h, and 24 h) as a function of residue number. Additional time points between 10 s and 24 h are presented in Figure S2. HX occurs throughout the solvent-exposed secondary structures to different extents depending on the local peptide backbone dynamics. The fraction deuterium incorporated into the domain is greatest in the N-terminus, $\beta 2$ loop (residues I₃₆–I₄₀), $\beta 4$ – $\beta 5$ hairpin (I₅₁–F₆₄), $\beta 8$ loop (Y₉₇–P₁₀₀), 3_{10} helix (A₁₀₂–L₁₀₈), and C-terminus. HX within helix $\alpha 1$ (residues E₁₂₄–Q₁₄₂) is minimal, and residues in helix $\alpha 2$ (A₁₅₂–R₁₆₂) do not exchange at all, indicating that these helices are stable. The time dependence of incorporation of deuterium into specific residues in the various secondary structure regions of AraC is presented in Figures S3 and S4.

Here, we focus on the structural regions whose dynamics respond to the binding of arabinose. Figure 2 shows that HX of much of the domain remains the same in the apo and arabinose-bound states, but in three structural regions of the domain, the kinetics of exchange were clearly different in the presence and absence of arabinose. These regions include two sides of the arabinose binding barrel, (1) the $\beta 4$ – $\beta 5$ hairpin (I₅₁–F₆₄) and (2) the loop between strand $\beta 8$ and the 3_{10} helix adjacent in tertiary structure to Ala₁₇ in the N-terminal arm. The C-terminal interdomain linker, partially resolved in various crystal structures of the dimerization domain, is also responsive to arabinose binding.

Simultaneous Stabilization and Relaxation of the Arabinose Binding Barrel.

Figures 3 and 4 illustrate the dynamics of exchange in the arabinose binding barrel in greater detail. In Figure 3, the $\beta 4$ – $\beta 5$ hairpin loop (residues I₅₁–F₆₄)

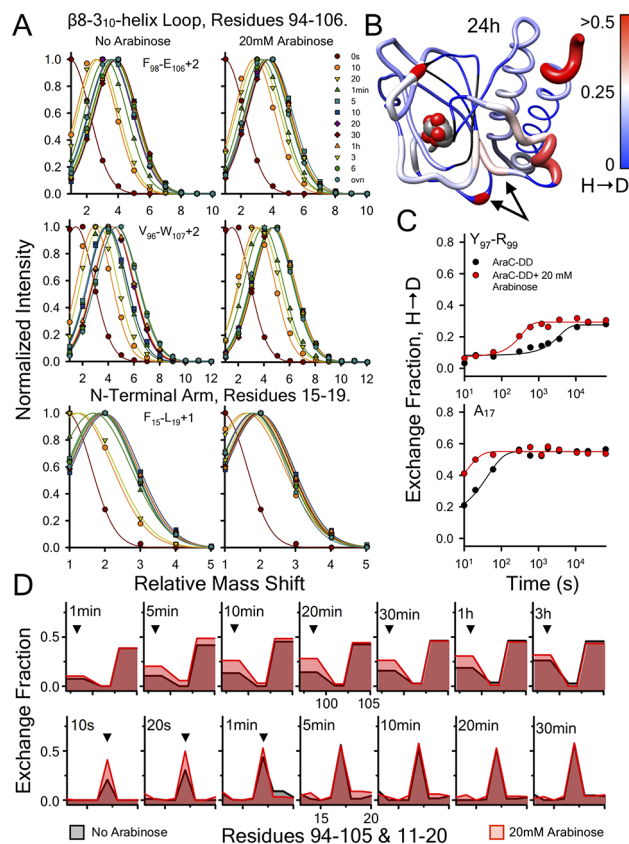


Figure 4. Arabinose binding enhances the hydrogen exchange in residues Y₉₇–R₉₉ and A₁₇ connected through space in the $\beta 8$ – 3_{10} loop and the N-terminus, respectively. HXMS was quantified in triplicate at times between 10 s to 6 h and 24 h. (A) Peptide envelopes (normalized intensity vs mass shift relative to the “all H” peak) of three peptides covering the region: top, F₉₈–E₁₀₆, charge state of +2; middle, V₉₆–W₁₀₇, charge state of +2; bottom, F₁₅–L₁₉, charge state of +1. (B) Hydrogen–deuterium exchange fraction mapped onto the structure of AraC (PDB entry 2ARC⁸): black, not resolved; blue, 0; white, 0.25; red, ≥ 0.5 . Rendered using UCSF Chimera.⁴³ Arrows indicate the structural location of this region. (C) HX kinetics of site-resolved Y₉₇–R₉₉ and A₁₇ residues are observed to be faster in the presence of arabinose than in its absence. (D) HX kinetics of the region including and surrounding Y₉₇–R₉₉ between 1 min and 3 h and A₁₇ between 10 s and 30 min illustrate localized HX kinetics. Arrowheads indicate the residues involved in the altered kinetics.

is observed to exchange less in the bound state than in the apo state, indicating that arabinose binding stabilizes this secondary structure region. The extent of incorporation of deuterium is observed to increase as a function of time in the apo state within specific peptides (T₅₀–E₆₃, G₅₃–E₆₃, and G₅₅–E₆₃) of this structural region causing a gradual shift in the relative mass. Conversely, the mass of these peptides remains comparably constant in the bound state (Figure 3A). Residues (I₅₁, G₅₅, V₅₆, and Q₆₀–E₆₃) in this structural region show the same gradual uptake of deuterium in the apo state relative to the bound state as a function of time (Figure 3B). Overall, the exchange of residues in the entire $\beta 4$ – $\beta 5$ hairpin loop increases faster in the apo state (Figure 3C), indicating that this loop readily samples open and closed conformations that, possibly, facilitate the binding of arabinose (Figure 3D). Once arabinose is bound, the closed conformation of this hairpin loop is stabilized and HX of the region is quenched.

In addition to the stabilization of the $\beta 4$ – $\beta 5$ hairpin loop caused by the binding of arabinose, residues on the opposite side of the binding barrel in the $\beta 8$ – 3_{10} loop and in A_{17} of the N-terminus (Figure 4B), each of which is adjacent in the three-dimensional structure of the domain, show increased exchange kinetics. Figure 4A shows that the relative masses of two peptides (F_{98} – E_{106} and V_{96} – W_{107}) in the $\beta 8$ – 3_{10} loop and one peptide (F_{15} – L_{19}) in the N-terminal arm are slightly shifted to higher masses as a function of time in the bound state. Closer examination of the kinetics of residues Y_{97} – R_{99} and A_{17} shows that the exchange is shifted to earlier times, indicating arabinose binding relaxes this region of the binding barrel, resulting in enhanced exchange rates (Figure 4C,D). Thus, the flexibility of this structural region is increased concomitant with stabilization of the $\beta 4$ – $\beta 5$ hairpin loop. None of the residue side chains in either the $\beta 4$ – $\beta 5$ hairpin loop, the $\beta 8$ – 3_{10} loop, or A_{17} make direct atomic interactions with arabinose and thus could also be considered to have allosteric effects within the binding barrel.

Allosteric Relaxation of the C-Terminal Interdomain Linker. In addition to changes in the exchange rates of residues lining the arabinose binding barrel, we also see alterations in exchange rates of more distant residues. Figure 5 illustrates that residues in the interdomain linker also relax in

response to arabinose binding. This is observed in a specific peptide spanning residues R_{161} – S_{169} , which incorporates deuterium faster in the bound state than in the apo state (Figure 5A). The exchange kinetics of residues are increased, resulting in a shift in the exchange fraction versus time to earlier time points (Figure 5B). This allosteric effect is highly localized to I_{167} and N_{168} as the surrounding residues exchange equally in the bound and apo states of the domain (Figure 5C).

Upon close inspection of the hydrogen-bonded structure of the C-terminal helix (B chain of PDB entry 2ARC, arabinose-bound state),⁸ it becomes evident that the helix is capped at the C-terminus by a hydrogen bond between the N_{168} side chain and the M_{164} carbonyl (Figure 5D). Following the nomenclature of Aurora and Rose,³⁴ residues prior to and including I_{167} (the C cap) follow the ($i \rightarrow i + 4$) traditional hydrogen bonding pattern of an α -helix and N_{168} is the first nonhelical residue, C' . Capping of carbonyls by side chains is less frequent than by backbone amides at helix C-termini,³⁴ but this cap redistributes the α -helix ($i \rightarrow i + 4$) hydrogen bonding pattern to ($i \rightarrow i + 3$) hydrogen bonds between the carbonyl of A_{166} and the amide of E_{169} and between the carbonyl of E_{165} and the amide of N_{168} where the helix terminates. Apo structures of AraC do not have N_{168} resolved, or N_{168} does not form a C cap motif.^{8,23} This suggests that formation of the C cap may be responsible for the enhanced exchange of residues I_{167} and N_{168} in the presence of arabinose. C capping specifically by asparagine has also been observed in other proteins using nuclear magnetic resonance (NMR).³⁵

Hydrogen–Deuterium Exchange of Full-Length AraC Confirms Observations in the Dimerization Domain and Reveals Allosteric Stabilization of the DNA Binding Domain. Figure 6A shows the exchange fraction of deuterium incorporated into the full-length AraC protein at three D_2O incubation times (10 s, 1 min, and 10 min) as a function of residue number. Additional time points between 10 s and 1 h are presented in Figure S5. The kinetics of incorporation of deuterium into the individual residues of different secondary structure regions of full-length AraC are presented in Figures S6 and S7. Longer D_2O incubation times resulted in the aggregation of AraC that caused loss of peptide coverage and resolution of the protein hydrogen exchange. This experimental complication was only marginally protected by the presence of bound arabinose and 20% glycerol³⁶ and is likely due to a kosmotropic effect of D_2O compared to water as the hydrogen bonding of D_2O is weaker than that of H_2O .³⁷ Hydrogen exchange at shorter incubation times was amenable to data analysis and interpretation.

Figure 6A illustrates that the level of HX within the DNA binding domain is significantly greater than that of the dimerization domain. The NMR solution structure of the AraC DNA binding domain is comprised of seven α -helices.³⁸ The enhanced HX of the DNA binding domain indicates that it is less stable than the dimerization domain, certainly more dynamic, or even partially disordered because the α -helices are exchanging very rapidly throughout the DNA binding domain structure (Figure 6B).

Although the stabilization of the $\beta 4$ – $\beta 5$ hairpin loop by arabinose binding was not observed in the full-length protein in the short time range of 10 s to 30 min, relaxation of the arabinose binding barrel and the interdomain linker was observed. Figure 6C illustrates these observations with two peptides: F_{98} – E_{106} in the $\beta 8$ – 3_{10} loop and R_{161} – S_{169} in the

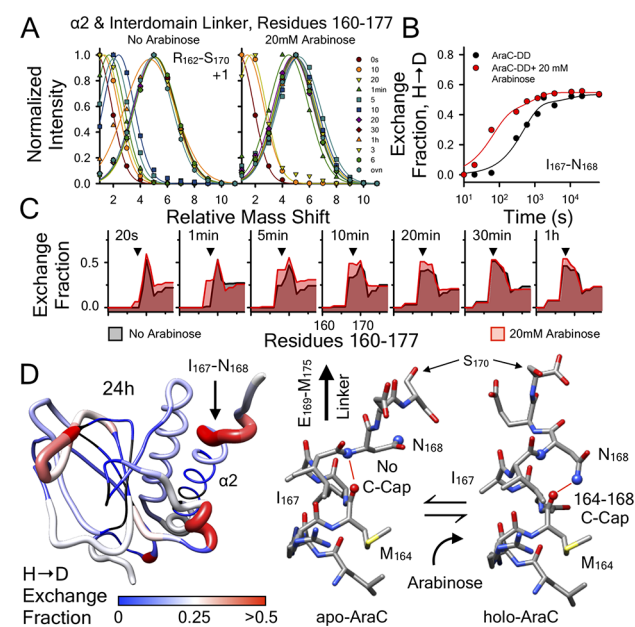


Figure 5. Arabinose binding enhances hydrogen exchange in residues I_{167} and N_{168} of the C-terminal linker of the dimerization domain. HXMS was quantified in triplicate at times between 10 s to 6 h and 24 h. (A) Peptide envelopes (normalized intensity vs mass shift relative to the “all H” peak) of the R_{161} – S_{169} peptide at a charge state of +1. (B) HX kinetics of site-resolved residues I_{167} and N_{168} of the C-terminal linker are observed to be faster in the presence of arabinose than in its absence. (C) HX kinetics of the region including and surrounding I_{167} and N_{168} between 20 s and 1 h illustrate the difference in HX kinetics is localized to I_{167} and N_{168} with only moderate differences in the surrounding residues. Arrowheads indicate the residues I_{167} and N_{168} involved in the altered kinetics. (D) Hydrogen–deuterium exchange fraction mapped onto the apo structure of AraC (PDB entry 1XJA²³) and potential C-terminal cap equilibrium of helix $\alpha 2$ containing residues I_{167} and N_{168} . Structures of the C-termini of apo-AraC (PDB entry 1XJA²³) and holo-AraC (PDB entry 2ARC⁸) of the $\alpha 2$ helix interdomain linker junction.

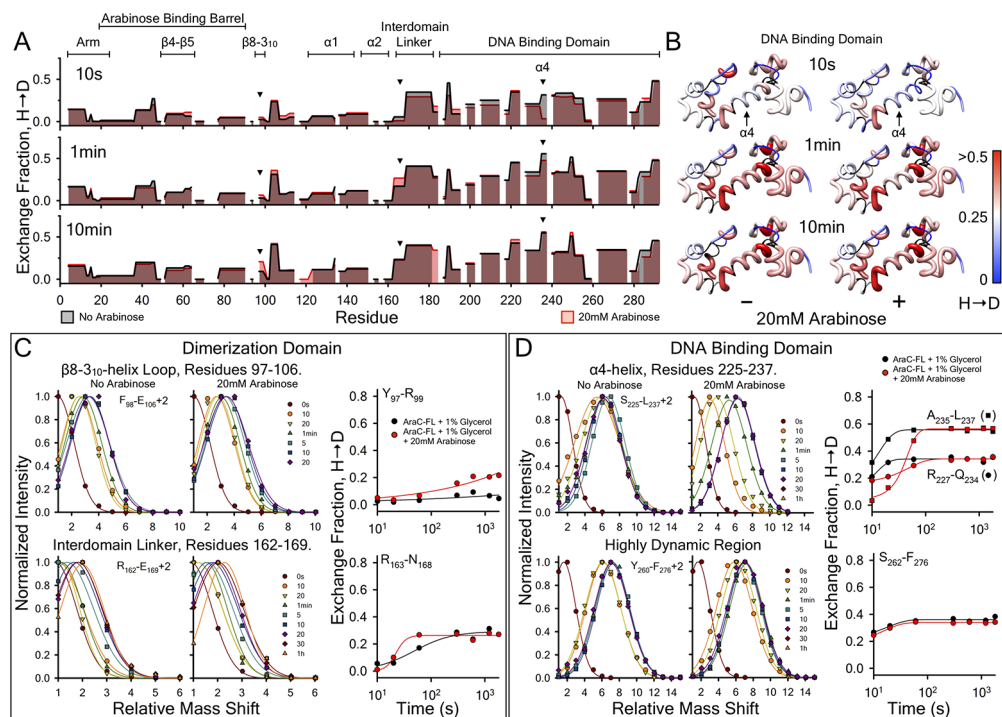


Figure 6. (A) Comparison of the hydrogen exchange of the full-length AraC protein in the presence (red) and absence (black) of 20 mM arabinose as a function of residue number throughout the protein at three exchange time points: 10 s (top), 1 min (middle), and 10 min (bottom). HXMS was quantified in triplicate at each exchange time point. (B) Hydrogen–deuterium exchange fraction mapped onto the structure of the AraC DNA binding domain (PDB entry 2K9S²⁸): black, not resolved; blue, 0; white, 0.25; red, ≥ 0.5 . Rendered using UCSF Chimera.²⁷ (C) Peptide envelopes (normalized intensity vs mass shift relative to the “all H” peak) of two peptides covering the dimerization domain in full-length AraC that confirm observations in the dimerization domain (Figures 4 and 5): top, F₉₈–E₁₀₆, charge state of +2; bottom, R₁₆₂–N₁₆₉, charge state of +2. HX kinetics of site-resolved Y₉₇–R₉₉ and R₁₆₂–N₁₆₈ residues are observed to be faster in the presence of arabinose than in its absence. (D) Peptide envelopes of two peptides covering the DNA binding domain in full-length AraC: top, S₂₂₅–L₂₃₇, charge state of +2; bottom, Y₂₆₀–F₂₇₆, charge state of +2. HX kinetics of site-resolved residues in $\alpha 4$, A₂₃₅–L₂₃₇ and R₂₂₇–N₂₃₄, are observed to be slower in the presence of arabinose than in its absence. S₂₆₂–L₂₇₆ have fully exchanged in 1 min.

interdomain linker. The difference between the relative mass shifts of these peptides in the presence and absence of arabinose as a function of time is subtle, but the exchange of individual residues reveals enhanced uptake of deuterium in residues Y₉₇–R₉₉ of the $\beta 8$ – $\beta 10$ loop and a kinetic shift of deuterium incorporation in residues R₁₆₃–N₁₆₈ of the interdomain linker. These observations confirm that the intrinsic conformational dynamics of the dimerization domain alone also apply to the full-length AraC protein containing the DNA binding domain.

Despite the high exchange rates seen in the DNA binding domain, it was possible to see a significant reduction in the exchange rates of residues in helix $\alpha 4$ caused by the presence of arabinose. The relative mass shifts of residues S₂₂₅–L₂₃₇ in the top panel of Figure 6D demonstrate that incorporation of deuterium into helix $\alpha 4$ is faster in the absence of arabinose. Site-resolved regions A₂₃₅–L₂₃₇ and R₂₂₇–Q₂₃₄ also show a kinetic delay of the exchange reaction in the presence of arabinose. Comparatively, residues S₂₆₂–F₂₇₆ of C-terminal peptide Y₂₆₀–F₂₇₆ derived from helices $\alpha 6$ and $\alpha 7$ are highly dynamic with no observed change induced by arabinose.

DISCUSSION

Here, we have described hydrogen–deuterium exchange experiments designed to identify which structural regions of AraC respond to arabinose binding. HXMS was performed as a function of time between 10 s and 24 h to assess the kinetics of exchange in the dimerization domain with the interdomain

linker and full-length AraC, containing the dimerization and DNA binding domains. Two features are notable in this comparative study of AraC in the presence and absence of excess arabinose. (1) HX differences are observed in residues of the arabinose binding dimerization domain that confirm arabinose is bound. (2) As expected for an allosteric protein, arabinose-induced changes in HX dynamics are observed both adjacent to the bound arabinose and at more distant locations in the protein.

Arabinose binding directly affects the exchange dynamics of residues surrounding the arabinose binding pocket. HXMS detects a quenching of the hydrogen–deuterium exchange in residues of the $\beta 4$ – $\beta 5$ hairpin loop (I₅₁–F₆₄) near the top of the arabinose binding β -barrel (Figure 3), indicating a stabilization of this region of the dimerization domain when arabinose is bound. A moderate enhancement of the exchange kinetics is observed in residue A₁₇ of the N-terminal arm and in residues V₉₆–W₁₀₇ of the $\beta 8$ – $\beta 10$ loop (Figure 4). This may reflect a repositioning of the N-terminal arm of the dimerization domain as is observed in crystal structures.^{21,23} However, other than that observed for A₁₇, there is no detectable difference in the exchange of residues of the N-terminal arm in the time range measured. Exchange in residues 4–12 is complete by 10 s, and residues 13–16 are stable and do not exchange regardless of whether arabinose is bound (Figure S3). Moreover, the N-terminus is unaffected by arabinose in full-length AraC containing the DNA binding domain (Figure S6).

The physiological and biochemical behavior of polyalanine and polyglycine linker substitutions¹ and proline mutations at different positions of the interdomain linker as well as insertions and deletions in the linker^{26,27} has suggested that, in the absence of arabinose, the linker is helical, and we hypothesize that arabinose binding induces a helix–coil transition that provides the flexibility necessary for the protein to tightly bind to adjacent half-sites and activate transcription. The HXMS experiments reported here do not provide evidence supporting the helix–coil hypothesis because the extent of exchange within linker residues E₁₆₉–H₁₇₂ is not substantially different between the arabinose-bound and unbound states. However, arabinose binding does result in highly localized differences in exchange kinetics at the beginning of the interdomain linker starting at the C-terminal end of helix $\alpha 2$ of the dimerization domain.

As mentioned above, the exchange rates of residues I₁₆₇ and N₁₆₈ are significantly increased when arabinose is bound (Figure 5). One mechanism that might account for this is an arabinose-induced formation of a C-terminal helix cap by the asparagine resulting from weakened amide hydrogen bonds at the end of helix $\alpha 2$. Similar enhanced HX has been previously observed by NMR in a destabilized helix N capping box of helix G of the C lobe of cardiac troponin C upon binding of the phosphomimetic N domain of troponin I.³⁹ A C-terminal helix capping motif terminating helix $\alpha 2$ of the AraC dimerization domain in the presence of arabinose could increase the level of freedom of several of the peptide backbone dihedral angles of residues following the N₁₆₈ C cap motif and allow AraC to more easily adopt the inducing conformation. Several facts argue in favor of this interpretation. First, asparagine is one of the strongest C-terminal capping residues.^{34,35} Second, in the crystal structures of the AraC dimerization domain with and without arabinose bound, C-terminal capping occurs only in the protein crystallized in the presence of arabinose.

It should be noted that a somewhat elevated rate of exchange was also observed at residues I₁₆₇ and N₁₆₈ even in the absence of arabinose. It is possible, therefore, that the side chain of N₁₆₈ is in an equilibrium between a capped state and an uncapped state so that exchange can occur in the absence of arabinose and that the binding of arabinose raises the probability of the capped state. This flickering between the normal helix hydrogen bonding and the side chain capping of the dimerizing helix might allow for a modulation of the length of helix $\alpha 2$ or the linker region just beyond a few residues and serve to regulate the strength by which the DNA binding domains are held in positions favorable for DNA looping and repression.

In these experiments, the binding of arabinose to the dimerization domain also decreases the rate of exchange of multiple residues in the DNA binding domain, particularly in the domain's central α helix that supports the two helix–turn–helix DNA binding motifs. This must result from an altered DNA binding domain–dimerization interaction. Whether this is a result of a domain–domain interaction that occurs only in the presence or only in the absence of arabinose or whether arabinose changes interactions that occur in both states cannot be determined with the current data. It should be noted, however, that multiple lines of physical evidence exist for an interaction that occurs in the presence of arabinose.⁴⁰ Similarly, co-varying amino acid residues in the dimerization domain and DNA binding domain in AraC homologues⁴¹

occur only in positions compatible with the positioning of the DNA binding domains that is required for induction.

In conclusion, these HXMS studies of the WT sequence of AraC demonstrate that the binding of arabinose induces highly localized changes in H–D exchange rates allosteric to the binding site. These effects do not appear to involve any substantial unfolding of the protein but are consistent with the formation of a C-terminal helix cap of the dimerization domain of helix $\alpha 2$. Although the mechanism of transmission of the signal to the responsive residues that arabinose has bound remains undetermined, such an allosteric effect on the backbone hydrogen bonding stability of residues at the junction between helix $\alpha 2$ and the interdomain linker would allow the DNA binding domains to unhinge and accommodate alternative DNA binding configurations commensurate with transcription activation of *araCBAD*.^{12,15,42}

■ ASSOCIATED CONTENT

📄 Supporting Information

The Supporting Information is available free of charge on the ACS Publications website at DOI: 10.1021/acs.biochem.9b00389.

Peptide mapping and time dependence of hydrogen–deuterium exchange of the AraC dimerization domain and full-length AraC (PDF)

Accession Codes

AraC, UniProt accession number P0A9E0 (ARAC_ECOLI).

■ AUTHOR INFORMATION

Corresponding Authors

*E-mail: auton.matthew@mayo.edu.

*E-mail: rfschleif@jhu.edu.

ORCID

Matthew J. Brown: 0000-0003-3640-5379

Matthew Auton: 0000-0002-4446-6932

Author Contributions

A.T. performed and analyzed the HXMS experiments. M.J.B. expressed and purified the AraC dimerization domain and the full-length AraC protein. R.F.S. and M.A. designed the research. M.A. wrote the paper.

Notes

The authors declare no competing financial interest.

■ ACKNOWLEDGMENTS

The authors thank Dr. George Rose for encouragement and ongoing discussions over the years and Drs. S. Walter Englander and Leland Mayne for very helpful scientific discussions regarding optimization of HXMS and the establishment of HXMS technology in the Auton lab.

■ ABBREVIATIONS

HXMS, hydrogen–deuterium exchange mass spectrometry; PDB, Protein Data Bank.

■ REFERENCES

- (1) Brown, M., and Schleif, R. F. (2019) Helical Behavior of the Interdomain Linker of the Escherichia coli AraC Protein. *Biochemistry*, DOI: 10.1021/acs.biochem.9b00234.
- (2) Steffen, D., and Schleif, R. (1977) In vitro construction of plasmids which result in overproduction of the protein product of the *araC* gene of Escherichia coli. *Mol. Gen. Genet.* 157, 341–344.

- (3) Hendrickson, W., and Schleif, R. (1985) A dimer of AraC protein contacts three adjacent major groove regions of the araI DNA site. *Proc. Natl. Acad. Sci. U. S. A.* 82, 3129–3133.
- (4) Bustos, S. A., and Schleif, R. F. (1993) Functional domains of the AraC protein. *Proc. Natl. Acad. Sci. U. S. A.* 90, 5638–5642.
- (5) Sheppard, D. E., and Englesberg, E. (1967) Further evidence for positive control of the L-arabinose system by gene araC. *J. Mol. Biol.* 25, 443–454.
- (6) Wilcox, G., Boulter, J., and Lee, N. (1974) Direction of transcription of the regulatory gene araC in *Escherichia coli* B-r. *Proc. Natl. Acad. Sci. U. S. A.* 71, 3635–3639.
- (7) Soisson, S. M., MacDougall-Shackleton, B., Schleif, R., and Wolberger, C. (1997) The 1.6 Å crystal structure of the AraC sugar-binding and dimerization domain complexed with D-fucose. *J. Mol. Biol.* 273, 226–237.
- (8) Soisson, S. M., MacDougall-Shackleton, B., Schleif, R., and Wolberger, C. (1997) Structural basis for ligand-regulated oligomerization of AraC. *Science* 276, 421–425.
- (9) Cole, S. D., and Schleif, R. (2012) A new and unexpected domain-domain interaction in the AraC protein. *Proteins: Struct., Funct., Genet.* 80, 1465–1475.
- (10) Eustance, R. J., and Schleif, R. F. (1996) The linker region of AraC protein. *J. Bacteriol.* 178, 7025–7030.
- (11) Eustance, R. J., Bustos, S. A., and Schleif, R. F. (1994) Reaching out. Locating and lengthening the interdomain linker in AraC protein. *J. Mol. Biol.* 242, 330–338.
- (12) Huo, L., Martin, K. J., and Schleif, R. (1988) Alternative DNA loops regulate the arabinose operon in *Escherichia coli*. *Proc. Natl. Acad. Sci. U. S. A.* 85, 5444–5448.
- (13) Dunn, T. M., Hahn, S., Ogden, S., and Schleif, R. F. (1984) An operator at –280 base pairs that is required for repression of araBAD operon promoter: addition of DNA helical turns between the operator and promoter cyclically hinders repression. *Proc. Natl. Acad. Sci. U. S. A.* 81, 5017–5020.
- (14) Casadaban, M. J. (1976) Regulation of the regulatory gene for the arabinose pathway, araC. *J. Mol. Biol.* 104, 557–566.
- (15) Hahn, S., and Schleif, R. (1983) In vivo regulation of the *Escherichia coli* araC promoter. *J. Bacteriol.* 155, 593–600.
- (16) Harmer, T., Wu, M., and Schleif, R. (2001) The role of rigidity in DNA looping-unlooping by AraC. *Proc. Natl. Acad. Sci. U. S. A.* 98, 427–431.
- (17) Hahn, S., Hendrickson, W., and Schleif, R. (1986) Transcription of *Escherichia coli* ara in vitro. The cyclic AMP receptor protein requirement for PBAD induction that depends on the presence and orientation of the araO2 site. *J. Mol. Biol.* 188, 355–367.
- (18) Borowiec, J. A., Zhang, L., Sasse-Dwight, S., and Gralla, J. D. (1987) DNA supercoiling promotes formation of a bent repression loop in lac DNA. *J. Mol. Biol.* 196, 101–111.
- (19) Carra, J. H., and Schleif, R. F. (1993) Variation of half-site organization and DNA looping by AraC protein. *EMBO J.* 12, 35–44.
- (20) Rodgers, M. E., Holder, N. D., Dirla, S., and Schleif, R. (2009) Functional modes of the regulatory arm of AraC. *Proteins: Struct., Funct., Genet.* 74, 81–91.
- (21) Schleif, R. (2010) AraC protein, regulation of the l-arabinose operon in *Escherichia coli*, and the light switch mechanism of AraC action. *FEMS Microbiol Rev.* 34, 779–796.
- (22) Saviola, B., Seabold, R., and Schleif, R. F. (1998) Arm-domain interactions in AraC. *J. Mol. Biol.* 278, 539–548.
- (23) Weldon, J. E., Rodgers, M. E., Larkin, C., and Schleif, R. F. (2007) Structure and properties of a truly apo form of AraC dimerization domain. *Proteins: Struct., Funct., Genet.* 66, 646–654.
- (24) Wu, M., and Schleif, R. (2001) Mapping arm-DNA-binding domain interactions in AraC. *J. Mol. Biol.* 307, 1001–1009.
- (25) Wu, M., and Schleif, R. (2001) Strengthened arm-dimerization domain interactions in AraC. *J. Biol. Chem.* 276, 2562–2564.
- (26) Seedorff, J., and Schleif, R. (2011) Active role of the interdomain linker of AraC. *J. Bacteriol.* 193, 5737–5746.
- (27) Malaga, F., Mayberry, O., Park, D. J., Rodgers, M. E., Toptygin, D., and Schleif, R. F. (2016) A genetic and physical study of the interdomain linker of *E. coli* AraC protein—a trans-subunit communication pathway. *Proteins: Struct., Funct., Genet.* 84, 448–460.
- (28) Mayne, L. (2016) Hydrogen Exchange Mass Spectrometry. *Methods Enzymol.* 566, 335–356.
- (29) Rodgers, M. E., and Schleif, R. (2012) Heterodimers reveal that two arabinose molecules are required for the normal arabinose response of AraC. *Biochemistry* 51, 8085–8091.
- (30) Tischer, A., Machha, V. R., Frontroth, J. P., Brehm, M. A., Obser, T., Schneppenheim, R., Mayne, L., Walter Englander, S., and Auton, M. (2017) Enhanced Local Disorder in a Clinically Elusive von Willebrand Factor Provokes High-Affinity Platelet Clumping. *J. Mol. Biol.* 429, 2161–2177.
- (31) Kan, Z. Y., Mayne, L., Sevugan Chetty, P., and Englander, S. W. (2011) ExMS: data analysis for HX-MS experiments. *J. Am. Soc. Mass Spectrom.* 22, 1906–1915.
- (32) Kan, Z. Y., Walters, B. T., Mayne, L., and Englander, S. W. (2013) Protein hydrogen exchange at residue resolution by proteolytic fragmentation mass spectrometry analysis. *Proc. Natl. Acad. Sci. U. S. A.* 110, 16438–16443.
- (33) Hendrickson, W., and Schleif, R. F. (1984) Regulation of the *Escherichia coli* L-arabinose operon studied by gel electrophoresis DNA binding assay. *J. Mol. Biol.* 178, 611–628.
- (34) Aurora, R., and Rose, G. D. (1998) Helix capping. *Protein Sci.* 7, 21–38.
- (35) Kallenbach, N. R., and Gong, Y. (1999) C-terminal capping motifs in model helical peptides. *Bioorg. Med. Chem.* 7, 143–151.
- (36) Auton, M., Rösger, J., Sinev, M., Holthausen, L. M., and Bolen, D. W. (2011) Osmolyte effects on protein stability and solubility: a balancing act between backbone and side-chains. *Biophys. Chem.* 159, 90–99.
- (37) Schott, H. (1988) Direct comparison of the strength of hydrogen bonds formed by H₂O and D₂O. *J. Macromol. Sci., Part B: Phys.* 27, 119–123.
- (38) Rodgers, M. E., and Schleif, R. (2009) Solution structure of the DNA binding domain of AraC protein. *Proteins: Struct., Funct., Genet.* 77, 202–208.
- (39) Finley, N. L., and Rosevear, P. R. (2004) Introduction of negative charge mimicking protein kinase C phosphorylation of cardiac troponin I. Effects on cardiac troponin C. *J. Biol. Chem.* 279, 54833–54840.
- (40) Dirla, S., Chien, J. Y., and Schleif, R. (2009) Constitutive mutations in the *Escherichia coli* AraC protein. *J. Bacteriol.* 191, 2668–2674.
- (41) Brown, M. (2019) The Allosteric Control Mechanism of AraC. Ph.D. Thesis, Department of Biology, Johns Hopkins University, Baltimore.
- (42) Brunelle, A., and Schleif, R. (1989) Determining residue-base interactions between AraC protein and araI DNA. *J. Mol. Biol.* 209, 607–622.
- (43) Pettersen, E. F., Goddard, T. D., Huang, C. C., Couch, G. S., Greenblatt, D. M., Meng, E. C., and Ferrin, T. E. (2004) UCSF Chimera—a visualization system for exploratory research and analysis. *J. Comput. Chem.* 25, 1605–1612.